Supporting Information

Enzymatic single-molecule kinetic isotope effects

Christopher R. Pudney[1], Richard S.K. Lane[2], Alistair J. Fielding[2], Steven W. Magennis[2], Sam Hay[1] and Nigel S. Scrutton[1]

[1]Manchester Interdisciplinary Biocentre, Faculty of Life Sciences, University of Manchester, 131 Princess Street, Manchester, M1 7DN, UK.

[2]The Photon Science Institute, School of Chemistry, University of Manchester, Oxford Road, Manchester M13 9PL, UK

Supplement to Results and Discussion

Choice of SM tracks. At the SM level, extrinsic fluorophores may show a variety of blinking behaviours such as triplet-state formation and photo-induced isomerization events. Alexa 488 does not undergo such isomerizations as there is no *cis*/*trans* stereoisomer. Further, in SM experiments where the protein-dye conjugate is immobilised, the observation of blinking behaviour may be complicated by the transient binding and dissociating of the conjugate from the surface of the coverslip. In the present system we do not find a large incidence of dye blinking in our SM tracks (< 10 %) and we do not analyse these tracks in the manner described below. This provides confidence that the observed transitions do not reflect photo-physical artefacts or transient binding interactions.

SM data fitting. From Figure 2C it is clear that there is a multi-component SM fluorescence signal attributable to the enzyme-dye construct. Below are the fitting statics (Table S1) for the enzyme only SM fluorescence intensity (ΔEm) data (Figure 2D). Data are fit as described in the main manuscript. The reported statistical values represent adjusted R^2 (adj.R^2) values extracted using Origin 8.5 software with a value closer to unity represents an improvement in fit. The data are split into fits where no parameters from Eq 1 were fixed (left) and where the fitting parameters (mid-point and width, not area) of 2 Gaussian fits derived from enzyme only data are fixed (right) to account for the enzyme only signal. From Table S1, the enzyme only data fit appropriately with 2 Gaussian components, additional Gaussians decrease the value of adj.R^2 suggesting more than 2 Gaussians over-parameterizes the data.

To identify additional components attributable to enzyme turnover, we have extracted the binned SM intensity data for enzyme + coenzyme (NADH/(*R*)-[4-^{2}H]-NADH), expressed as variance

from the mean intensity (ΔEm = Em – <Em>) as shown in Figure S3. A Mann-Whitney U test of enzyme and enzyme + coenzyme ΔEm data suggests no difference between enzyme only and substrate turnover (NADH, P_1 = 0.47 and (*R*)-[4-^{2}H]-NADH, P_1= 0.36). However, the fit to the NADH/(*R*)-[4-^{2}H]-NADH) data improves with the addition of more Gaussian components. Using the enzyme only data fixed for a 2 Gaussian fit (*n* = 2; Eq 1) gives a poorer fit for both NADH and (*R*)-[4-^{2}H]-NADH (adj.R^2 = 0.83/0.89) compared to the enzyme alone (adj.R^2 = 0.94). This suggests the enzyme data alone does not account for the SM turnover ΔEm values for NADH/(*R*)-[4-^{2}H]-NADH). Additional Gaussian components improve the NADH/(*R*)-[4-^{2}H]-NADH fit significantly. This argues that additional signal(s) should be taken into account beyond the 2 Gaussian components attributable to the enzyme only signal, particularly for the log *k* distributions with the NADH/(*R*)-[4-^{2}H]-NADH.

Further evidence for fitting extra components to the log *k* distributions arises from the magnitude of the extracted mid-point KIE values. Fitting both the NADH and (*R*)-[4-^{2}H]-NADH log *k* data to an *n* = 2 function (Eq 1) gives rise to KIE values of 1.8 ± 0.1 (for the major component by area) and 1.0 ± 0.01. These KIE values do not compare favourably with the ensemble KIE value (6.8 ± 0.4). However, fitting to an *n* = 3 function (Eq 1) with mid-point and width of the first two Gaussians fixed to account for the PETNR-Alexa-488 alone signal, gives a KIE of 3.7 ± 4.2. Clearly this value is much closer to the measured ensemble KIE and provides additional rationale beyond the fitting statistics of the ΔEm values (Figure S3) for the data fitting of log *k* values in the main manuscript.

FMN oxidation by molecular oxygen. We have also monitored FMN oxidation by molecular oxygen, with NADH and (*R*)-[4-^{2}H]-NADH as the reductant shown in Figure S4B. The rate constants for FMN oxidation by molecular oxygen in air-saturated water at room temperature is

$< 0.2\ s^{-1}$ and thus largely outside the detectable range of our single molecule experiment. Indeed, the extracted $f(\log k)$ distributions are adequately fit using the parameters for enzyme only dye intensity fluctuation (Figure 5 in the main text). In essence, many of the SM trajectories analyzed in this study contain only a single PETNR reduction, with no re-oxidation. However, we note that we do not expect a significant KIE on FMN oxidation. This then serves as a further control that our single molecule distributions for FMN reduction accurately reflect chemical turnover deconvolved from other dynamic processes.

Model-free determination of SM KIEs. Figure S6 shows model single-molecule 'H' and 'D' data, generated by taking 10^6 random time samples with (multi)exponential distributions. While the binned log (τ) and log (1/ τ) data are non-symmetrical, these data are reasonably fit by a Gaussian function (dashed lines in panel C-E), giving a midpoint value which is within 12% of the expected value. Next we calculated the frequency data for the KIE shown in Figure S7. Figure S7 provides verification of the model free KIE matrix method described in *Methods* using model data. The KIE datasets were determined in the same way as the experimental data in the main manuscript: 10^3 pseudo-random samples from both the H and D data were taken and every combination of $\tau(D)/\tau(H)$ was calculated to give 10^6 individual KIE values (Figure S7; Panels A and B). Note that while the log(t) and log(k) distributions are not symmetrical, the KIE distributions are symmetrical and can be accurately fit using a Gaussian function.

Tables

Table S1. Comparison of adj.R^2 values extracted from fitting Eq 1 to SM Δf data.

	No fixed data			2 Gaussians fixed using enzyme only data (*m*,*w* Eq 1)		
n (Eq 1)	2	3	4	2	3	4
Enzyme only	0.93539	0.90239	0.94027	-	0.91224	0.90365
NADH	0.93141	0.96607	0.96812	0.82834	0.92374	0.92403
(*R*)-[4-^{2}H]-NADH	0.9526	0.9714	0.97852	0.88562	0.93582	0.96061

Table S2. Area of fitted Gaussian components from Eq 1.

n	PETNR-Alexa-488	NADH	(*R*)-[4-^{2}H]-NADH
1	84 ± 5	62 ± 8	43 ± 3
2	16 ± 5	10 ± 3	16 ± 4
3	-	28 ± 6	41 ± 2

Area expressed as percent.

Figures

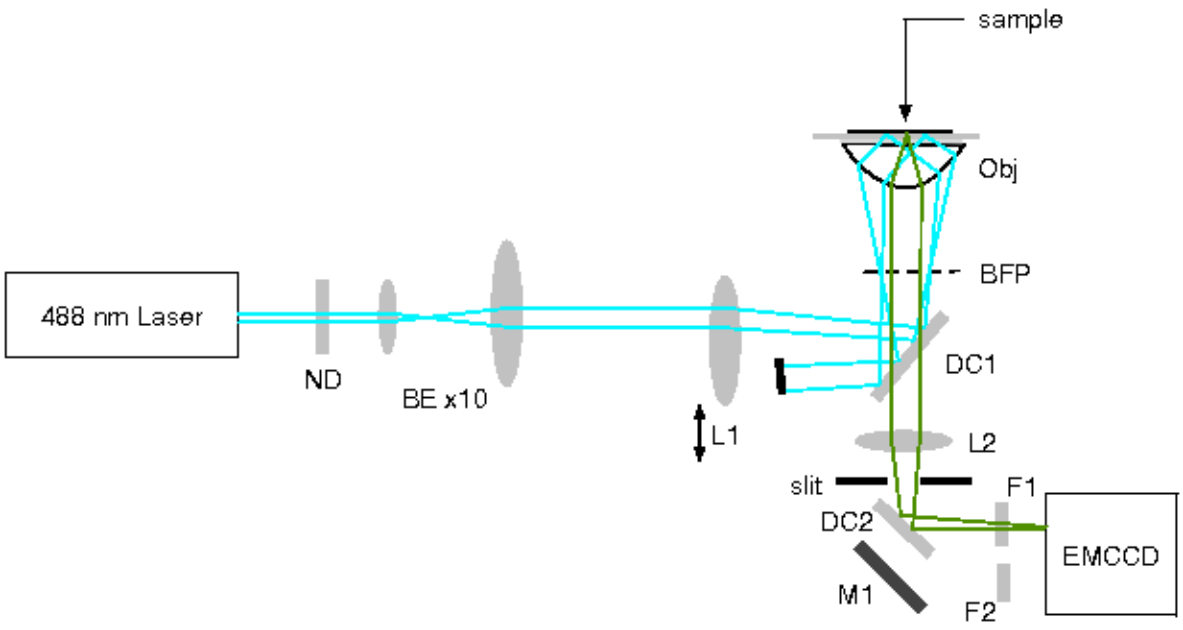

Figure S1. Schematic representation of the objective-type TIRF microscope. BE: beam expander, L1: f=400mm plano-convex lens with z-translation, ND: neutral density filters, Obj: microscope objective, M1: protected silver mirror, DC1-2: dichroic, cyan lines: laser light; green lines: fluorescence. F1-2: filters. See text for details.

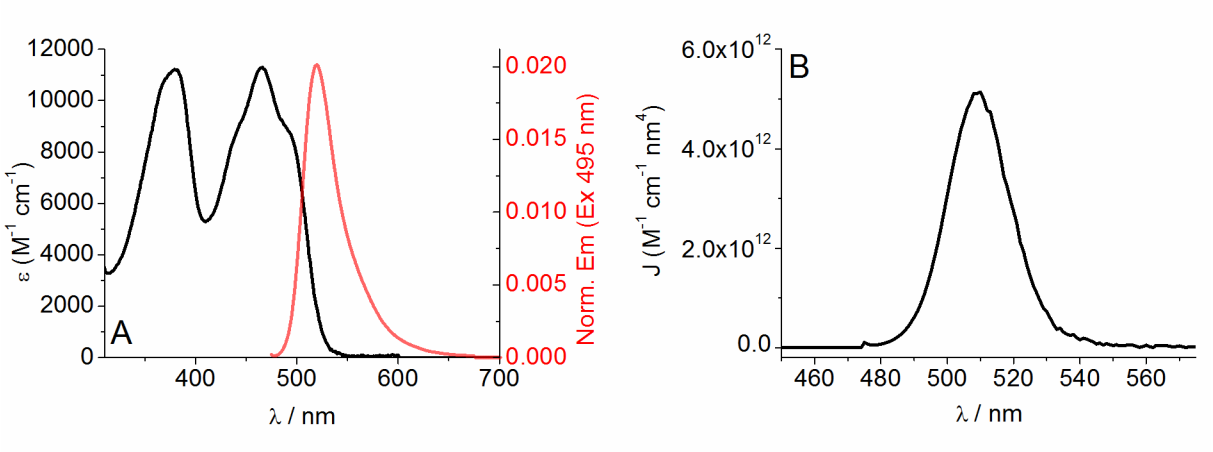

Figure S2. Spectral overlap of PETNR FMN moiety and Alexa-488. **(A)** Absorption spectrum of PETNR centered around the FMN absorbance (black line) and emission spectrum of Alexa-488 excited at 495 nm (red line). **(B)** Calculated spectral overlap of the spectra in **(A)**. The spectral overlap gives a Förster radius, $R_{0,}$ of 36.0 Å calculated by $R_0 = 0.2108[\kappa^2 \Phi_0 n^{-4} J]^{1/6}$, where κ^2 = 2/3, Φ_0 = 0.92, n = 1.33 and $J = 1.25 \times 10^{14}$ M^{-1} cm^{-1} nm^4.

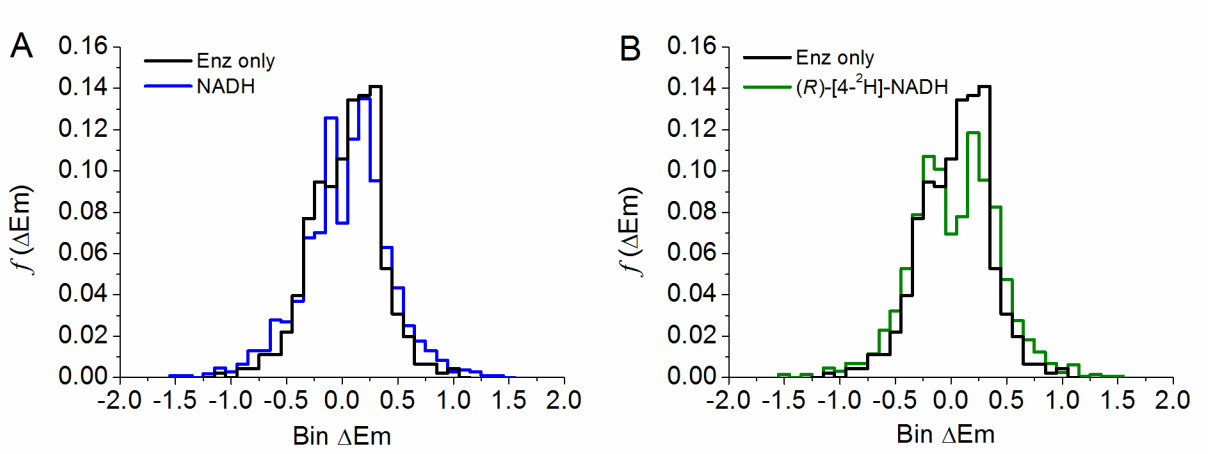

Figure S3. Comparison of SM fluorescence intensity fluctuations in PETNR-Alexa-488 (black line) with **(A)** NADH (blue line) and **(B)** (*R*)-[4-^{2}H]-NADH (green line).

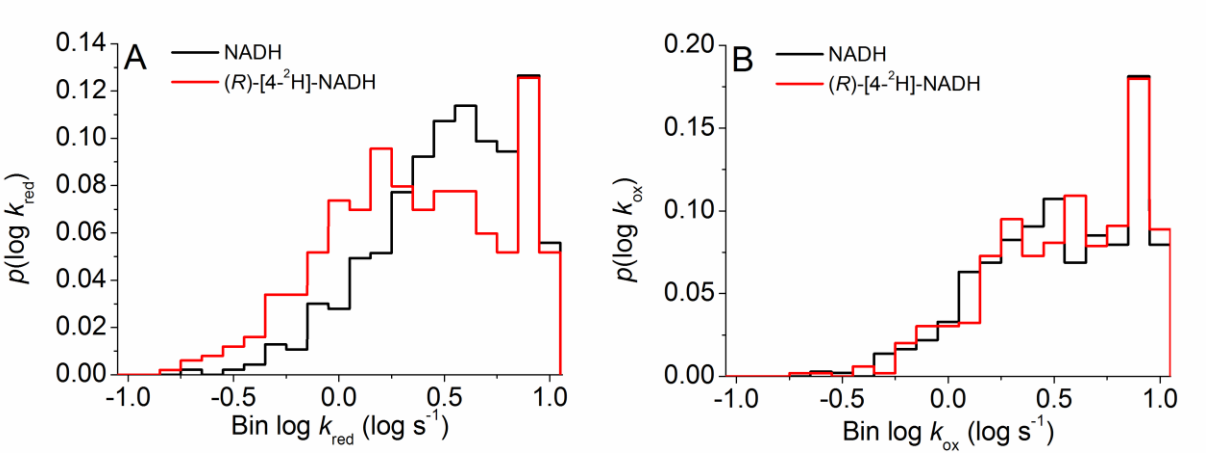

Figure S4. Comparison of the binned apparent rate constants extracted from SM traces for FMN reduction **(A)** and FMN oxidation **(B)**.

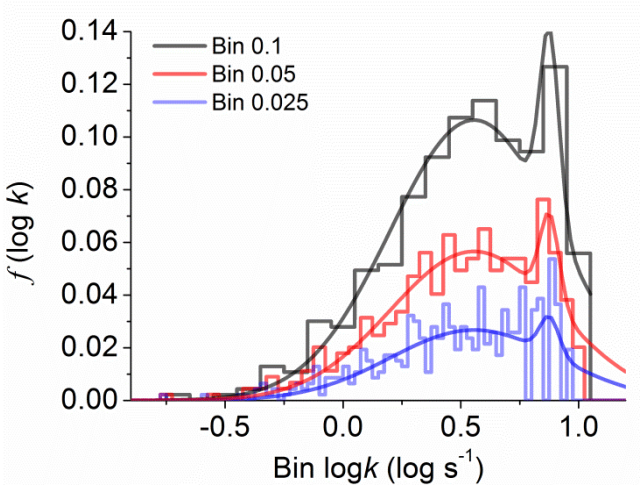

Figure S5. Example SM data fitting. For all SM data, several bin increments were simultaneously fit to the same multi-Gaussian function (Eq. 1, n = 2) shown in the figure as different colored solid lines. The midpoint and width of each Gaussian component is shared between bin intervals but the area of allowed to vary.

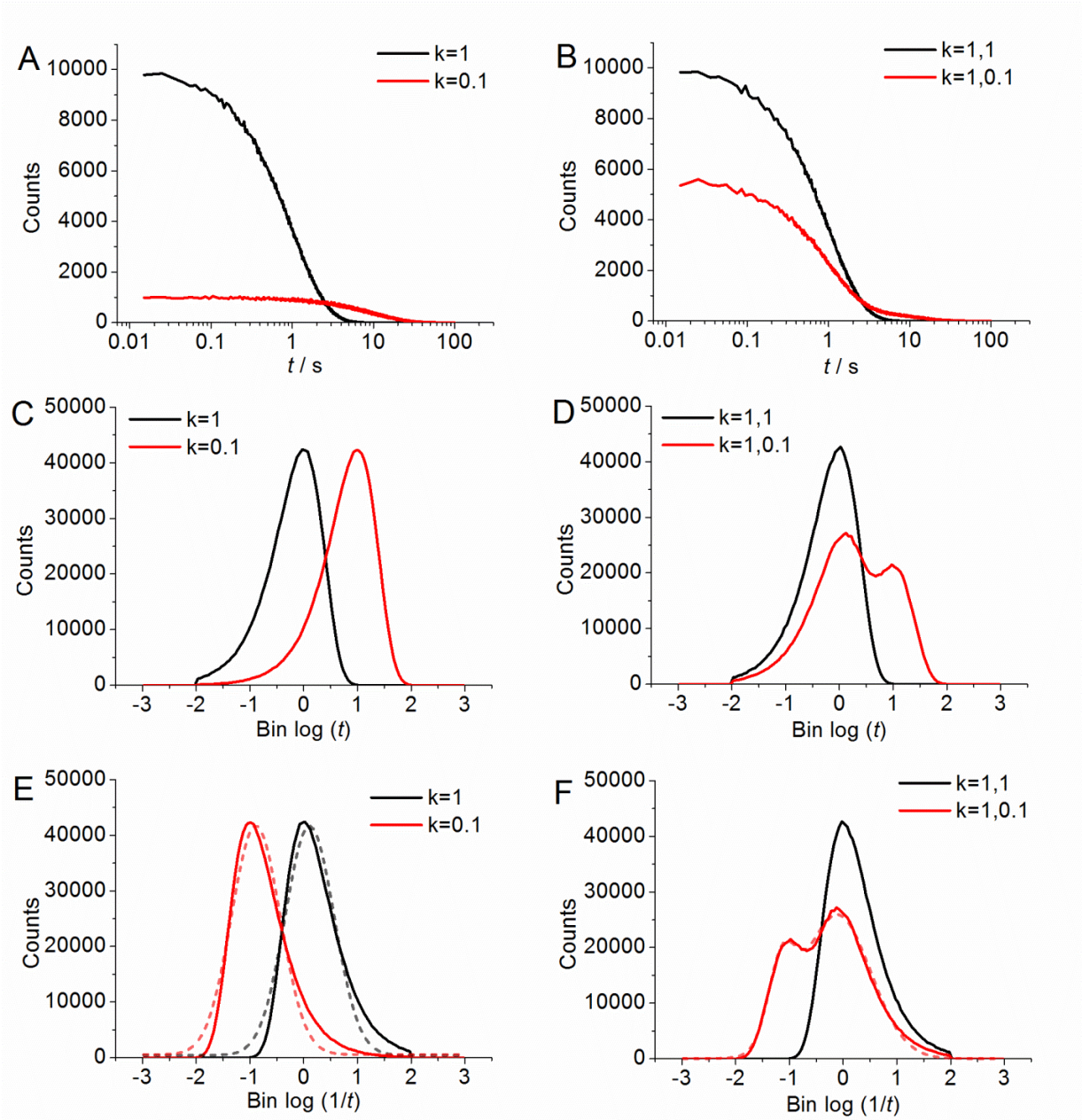

Figure S6. Modeling theoretical SM turnover data. Model data are shown for exponential decays (A) and double-exponential decays with equal amplitudes (B), 'dwell times' (C and D) and rate constant (E and F) for a KIE of 10 (A, C and E) and a KIE of 10and 1 (B, D and F). The dashed lines in E and F are fits to a single a double Gaussian function, respectively (dotted lines). In both cases the mid-points are within 12% of the theoretical rates. Note that black data in Panel F (k = 1, 1) has not been fit, but reflects the same case as for the black data in Panel E.

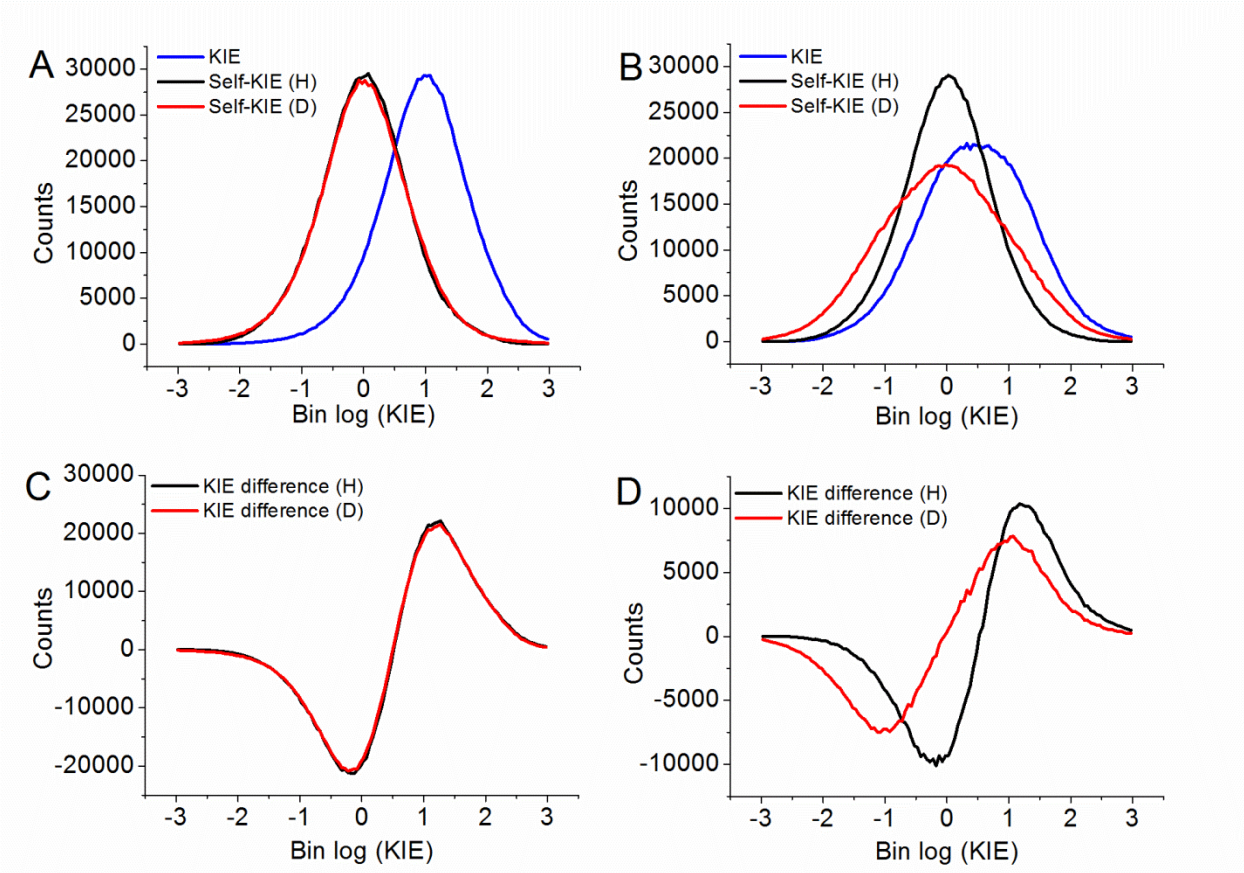

Figure S7. Modeling the theoretical SM KIE. The modeled data in Figure S6 was used to calculate KIE datasets using the same methods as described in the main text: blue in Panels A (KIE = 10) and B (KIE = 1 and 10). The red and black lines show the self-KIE, *i.e.* the same treatment for the H/H and D/D frequency data, respectively and panels C and D show the data after these self-KIEs have been subtracted from the H/D KIE dataset.

References

1 Pudney, C. R.; Hay, S.; Levy, C.; Sutclife, M.J.; Leys, D.; Scrutton, N.S. *J. Am. Chem. Soc.* **2009**, 131, 17072.